An Observer-Based Mechanical Sensor Failure Fault Tolerant Controller Structure in PMSM drive

Ahmad Akrad, Mickaël Hilairet, Demba Diallo
LGEP/SPEE Labs; CNRS UMR8507; SUPELEC; Univ Paris Sud-P11;
Univ Pierre et Marie Curie-P6; F-91192 Gif-sur-Yvette
(ahmad.akrad,mickael.hilairet,demba.diallo)@lgep.supelec.fr

***Abstract*—This paper presents a specific controller architecture devoted to obtain a Permanent Magnet Synchronous Motor drive robust to mechanical sensor failure. In order to increase the reliability which is a key issue in industrial and transportation applications (Electric or Hybrid ground vehicle or aerospace actuators) two virtual sensors (a two stage Extended Kalman Filter and a back-emf adaptive observer) and a voting algorithm are combined with the actual sensor to build a fault tolerant controller. The observers are evaluated off line with experimental data and the robustness against parameter variation is tested through simulation results. The Fault Tolerant Controller feasibility is proved through simulation of the PMSM drive.**

***Index Terms*—Permanent Magnet Synchronous Motors, position and speed estimation, sensorless drive, position sensor failure, fault tolerant controller.**

I. Introduction

Several failures afflict electrical motor drives and so far, redundant or conservative design has been used in every application where continuity of operations is a key feature. This is the case of home and civil appliances, such as, for example, air conditioning/heat pumps, engine cooling fans, and electric vehicles, where reliability is a key issue. Fault-tolerance has become an increasingly interesting topic in the last decade where the automation has become more complex. The objective is to give solutions that provide fault accomodation to the most frequent faults and thereby reduce the costs of handling the faults. In submerged pumps or hostile environments where accessibility to the drive and to the sensors is tedious and nevertheless continuity of operation is mandatory even in case of fault occurrence, a sensorless algorithm is indispensable to maintain the availability and therefore increase the reliability.

Due to its capability of field-weakening control, high efficiency, and high power density Permanent Magnet Synchronous Motors (PMSMs) are becoming competitive in many applications such as railway electric propulsion power train, EV or HEV [1], [2].

There are numerous study results about fault detection and fault-tolerant control [3]- [7], but most of them focused on the faults of power semiconductors of an inverter and stator windings of the motor. In [4], a fault tolerant controller for automotive applications with an induction machine has been presented. The proposed system adaptively changes of control technique in the event of sensor failure or recovery. In [5], a method to detect sensor faults and an algorithm to reconfigure the control system for interior permanent magnet motor drive have been described. The study focused on the detection of current sensor faults, the analysis of a current observer, and the resilient control of the drive system while retaining the same basic control strategy.

In this paper an active position sensor fault tolerant controller (FTC) is presented. It is based on the combination of the actual sensor and two virtual ones (a two stage Extended Kalman Filter and a back-emf adaptive observer). A voting algorithm (maximum likelihood) parameterized with reliability coefficients dedicated to each sensor on the whole speed range selects the appropriate input (speed and position) for the control loops [8].

The paper is composed of two sections. The first section is dedicated to the description of the sensorless algorithms and their experimental validation. The sensitivity analysis against parameter variation of the position and speed estimators is studied through intensive simulations. In the second section, the FTC architecture is introduced; the sensor and its faults are presented. The FTC is evaluated through simulation of the PMSM drive.

II. Position and speed observers

PMSM drive research has been concentrated on the elimination of the mechanical sensors at the motor shaft without deteriorating the dynamic performance of the drive-control system [9]- [12]. The advantages of sensorless AC drives are the lower cost, reduced size of the motor set, cable elimination, and increased reliability [13].

The position and speed estimations are computed by an Optimal Two-Stage Extended Kalman Filter (OTSEKF) and a back-emf adaptive observer (AO). The first observer is designed in the (dq) rotating frame, while the second one is based on a model in the $(\alpha\beta)$ reference frame.

A. Two-stage Extended Kalman filter

1) Continuous motor model: The salient PMSM is modeled in the standard (dq) reference frame as follows :

$$\begin{array}{rcl} \frac{d}{dt}X(t) & = & A_c(\Theta)\,X(t) + B_c^u(\Theta)\,U(t) + B_c^\Theta(\Theta)\,\Theta(t) \\ Y(t) & = & C(\Theta)\,X(t) \end{array} \quad (1)$$

978-1-4244-4252-2/09/$25.00 ©2009 IEEE

with

$$
\begin{aligned}
X &= \left[\begin{array}{cc} i_{sd} & i_{sq} \end{array}\right]^t \qquad \Theta = \left[\begin{array}{cc} \omega & \theta \end{array}\right]^t \\
U &= \left[\begin{array}{cc} v_{s\alpha} & v_{s\beta} \end{array}\right]^t \qquad Y = \left[\begin{array}{cc} i_{s\alpha} & i_{s\beta} \end{array}\right]^t \\
A_c(\Theta) &= \left[\begin{array}{cc} -\frac{R_s}{L_d} & \frac{\omega L_q}{L_d} \\ -\frac{\omega L_d}{L_q} & -\frac{R_s}{L_q} \end{array}\right] \\
B_c^u(\Theta) &= \left[\begin{array}{cc} \frac{cos(\theta)}{L_d} & \frac{sin(\theta)}{L_d} \\ -\frac{sin(\theta)}{L_q} & \frac{cos(\theta)}{L_q} \end{array}\right] \quad B_c^\Theta(\Theta) = \left[\begin{array}{cc} 0 & 0 \\ -\frac{\Phi}{L_q} & 0 \end{array}\right] \\
C(\Theta) &= \left[\begin{array}{cc} cos(\theta) & -sin(\theta) \\ sin(\theta) & cos(\theta) \end{array}\right]
\end{aligned}
$$

In these equations $v_{s\alpha}, v_{s\beta}, i_{s\alpha}, i_{s\beta}$ are the voltages and currents in the $(\alpha\beta)$ reference frame, i_{sd}, i_{sq} are currents in the (dq) frame, L_d and L_q are the stator inductances, R_s is the stator winding resistance, and ϕ is the flux produced by the magnets. The angular velocity ω is measured in electrical radians per second (the connection between electrical and mechanical variables is $\omega = P\Omega$, where P is the number of pole pairs) and θ is the electrical position.

2) Discretization of the motor model: For the digital implementation of an estimator, a discrete-time state space model is required. Provided that the input vector U is nearly constant during a sampling period T_s ($T_s = 200\ \mu s$), the previous continuous model (1) leads to the following discrete-time state space model :

$$
\begin{aligned}
X[k+1] &= A(\Theta)\, X[k] + B^u(\Theta)\, U[k] + B^\Theta(\Theta)\, \Theta[k] \\
Y[k] &= C(\Theta)\, X[k]
\end{aligned} \tag{2}
$$

Tolerating a small discretization error, a first order series expansion of the matrix exponential is used :

$$
\begin{aligned}
e^{A_c\, T_s} &\approx A = I + A_c\, T_s \\
A_c^{-1}\, (e^{A_c\, T_s} - I)\, B_c &\approx B = T_s\, B_c
\end{aligned}
$$

This leads to :

$$
\begin{aligned}
A(\Theta) &= \left[\begin{array}{cc} 1 - \frac{R_s}{L_d} T_s & \frac{\omega L_q}{L_d} T_s \\ -\frac{\omega L_d}{L_q} T_s & 1 - \frac{R_s}{L_q} T_s \end{array}\right] \\
B^u(\Theta) &= \left[\begin{array}{cc} \frac{cos(\theta)}{L_d} T_s & \frac{sin(\theta)}{L_d} T_s \\ -\frac{sin(\theta)}{L_q} T_s & \frac{cos(\theta)}{L_q} T_s \end{array}\right] \\
B^\Theta(\Theta) &= \left[\begin{array}{cc} 0 & 0 \\ -\frac{\Phi}{L_q} T_s & 0 \end{array}\right]
\end{aligned}
$$

This discretised model will be used in the prediction step of the EKF which is designed to estimate the unknown vector Θ previously defined.

3) OTSEKF Algorithm: The main objective of the estimator is to determine the position and speed of the PMSM. Therefore, those two variables must be concatenated with the previous state vector X. This leads to an augmented observer with a state space vector composed of the currents, the speed and position. Treating $X[k]$ as the full order state and $\Theta[k]$ as the unknown states, the state space model is described by :

$$
\begin{aligned}
X^a[k+1] &= \overline{A}(\Theta[k]) X^a[k] + \overline{B}(\Theta[k])\, U[k] + W[k] \\
Y[k] &= \overline{C}(\Theta[k]) X^a[k] + B^y(\Theta[k])\, U[k] + \eta[k]
\end{aligned} \tag{3}
$$

with

$$
\begin{aligned}
X^a[k] &= \left[\begin{array}{c} X[k] \\ \Theta[k] \end{array}\right] \\
\overline{A}(\Theta[k]) &= \left[\begin{array}{cc} A(\Theta[k]) & B^\Theta(\Theta[k]) \\ 0 & G(\Theta[k]) \end{array}\right] \\
\overline{B}(\Theta[k]) &= \left[\begin{array}{c} B^u(\Theta[k]) \\ 0 \end{array}\right] \\
\overline{C}(\Theta[k]) &= \left[\begin{array}{cc} C(\Theta[k]) & D(\Theta[k]) \end{array}\right] \\
W[k] &= \left[\begin{array}{c} W^x[k] \\ W^\Theta[k] \end{array}\right]
\end{aligned}
$$

where $G(\Theta[k])$ describes the evolution of the unknown state variable Θ between two time samples. The process noises $W^x[k]$, $W^\Theta[k]$ and the measurement noise $\eta[k]$ have the appropriate properties [14].

The application of the EKF [14] to the non-linear state space model (3) is described as follows :

$$
\begin{aligned}
X^a[k|k-1] &= \overline{A}[k-1] X^a[k-1|k-1] \\
&+ \overline{B}[k-1] U[k-1] \\
P[k|k-1] &= \overline{F}[k-1] P[k-1|k-1] \overline{F}^t[k-1] \\
&+ Q[k-1] \\
K[k] &= P[k|k-1] \overline{H}^t[k] \\
&+ (\overline{H}[k] P[k|k-1] \overline{H}^t[k] + R[k])^{-1} \\
X^a[k|k] &= X^a[k|k-1] + K[k](Y[k] \\
&- \overline{H}[k] X^a[k|k-1] - B^y[k] U[k]) \\
P[k|k] &= P[k|k-1] - K[k] \overline{H}[k] P[k|k-1]
\end{aligned}
$$

with

$$
\begin{aligned}
\overline{F}[k] &= \left[\begin{array}{cc} F(\Theta[k]) & E(\Theta[k]) \\ 0 & G(\Theta[k]) \end{array}\right] \\
\overline{H}[k] &= \left[\begin{array}{cc} H_1(\Theta[k]) & H_2(\Theta[k]) \end{array}\right] \\
F(\Theta[k]) &= \frac{\partial}{\partial X}\Big(A(\Theta[k])\, X[k] + B^\Theta(\Theta[k])\, \Theta[k] \\
&+ B^u(\Theta[k])\, U[k] \Big) = A(\Theta[k]) \\
E(\Theta[k]) &= \frac{\partial}{\partial \Theta}\Big(A(\Theta[k])\, X[k] + B^\Theta(\Theta[k])\, \Theta[k] \\
&+ B^u(\Theta[k])\, U[k] \Big) \\
E(\Theta[k]) &= \left[\begin{array}{cc} \frac{i_{sq} L_q}{L_d} T_s & \frac{v_{sq}}{L_d} T_s \\ -\frac{\Phi}{L_q} T_s - \frac{i_{sd} L_d}{L_q} T_s & -\frac{v_{sd}}{L_q} T_s \end{array}\right] \\
G(\Theta[k]) &= \left[\begin{array}{cc} 1 & 0 \\ T_s & 1 \end{array}\right] \qquad D(\Theta[k]) = \left[\begin{array}{cc} 0 & 0 \\ 0 & 0 \end{array}\right] \\
H_1(\Theta[k]) &= \frac{\partial}{\partial X}\Big(C(\Theta[k])\, X[k] + D(\Theta[k])\, \Theta[k] \\
&+ B^y(\Theta[k])\, U[k] \Big) = C(\Theta[k]) \\
H_2(\Theta[k]) &= \frac{\partial}{\partial \Theta}\Big(C(\Theta[k])\, X[k] + D(\Theta[k])\, \Theta[k] \\
&+ B^y(\Theta[k])\, U[k] \Big)
\end{aligned}
$$

$$
\begin{aligned}
H_2(\Theta[k]) &= \begin{bmatrix} 0 & -sin(\theta)i_{sd} - cos(\theta)i_{sq} \\ 0 & cos(\theta)i_{sd} - sin(\theta)i_{sq} \end{bmatrix} \\
K[k] &= \begin{bmatrix} K^x[k] \\ K^\Theta[k] \end{bmatrix} \\
P[.] &= \begin{bmatrix} P^x[.] & P^{x\Theta}[.] \\ (P^{x\Theta}[.])^t & P^\Theta[.] \end{bmatrix} \\
Q[k] &= \begin{bmatrix} Q^x[k] & Q^{x\Theta}[k] \\ (Q^{x\Theta}[k])^t & Q^\Theta[k] \end{bmatrix}
\end{aligned}
$$

where, $v_{sd} = cos(\theta)v_{s\alpha} + sin(\theta)v_{s\beta}$, $v_{sq} = -sin(\theta)v_{s\alpha} + cos(\theta)v_{s\beta}$ are voltages in the (dq) frame.

The Extended Kalman filter (EKF) has a heavier computational cost with a rough implementation. The use of a two-stage Extended Kalman filter reduces the computation time by 21% by reducing the number of operations [16], while maintaining the same level of performance. The non-linear OTSEKF is derived from the original EKF algorithm by an appropriate transformation so that the variance-covariance matrices are block-diagonal [15]–[17].

B. Back-emf adaptive observer

1) Back-emf estimation: The equation in the $(\alpha\beta)$ coordinates can be derived from (1) as follows [18] :

$$
\begin{aligned}
\frac{d}{dt}\begin{bmatrix} i_{s\alpha} \\ i_{s\beta} \end{bmatrix} &= \frac{1}{L_d}\begin{bmatrix} -R_s & -\omega(L_d - L_q) \\ \omega(L_d - L_q) & -R_s \end{bmatrix}\begin{bmatrix} i_{s\alpha} \\ i_{s\beta} \end{bmatrix} \\
&+ \frac{1}{L_d}\begin{bmatrix} -1 & 0 \\ 0 & -1 \end{bmatrix}\begin{bmatrix} e_{s\alpha} \\ e_{s\beta} \end{bmatrix} + \frac{1}{L_d}\begin{bmatrix} v_{s\alpha} \\ v_{s\beta} \end{bmatrix} \quad (4)
\end{aligned}
$$

with

$$
e = \begin{bmatrix} e_{s\alpha} \\ e_{s\beta} \end{bmatrix} = ((L_d - L_q)(\omega i_{sd} - \dot{i}_{sq}) + \phi\omega)\begin{bmatrix} -\sin\theta \\ \cos\theta \end{bmatrix} \quad (5)
$$

where e is defined as an Extended Electromotive Force (EEMF).

The following disturbance observer of the electrical model (4) can be used to estimate the back-EEMF components $e_{s\alpha}$, $e_{s\beta}$, which can be regarded as constant or slowly variable disturbance in the electrical equations [21].

$$
\begin{aligned}
\frac{d}{dt}\begin{bmatrix} \hat{i}_{s\alpha} \\ \hat{e}_{s\alpha} \end{bmatrix} &= \frac{1}{L_d}\begin{bmatrix} -R_s & -1 \\ 0 & 0 \end{bmatrix}\begin{bmatrix} \hat{i}_{s\alpha} \\ \hat{e}_{s\alpha} \end{bmatrix} + \begin{bmatrix} k_{\alpha 1} \\ k_{\alpha 2} \end{bmatrix}\tilde{i}_{s\alpha} \\
&+ \frac{1}{L_d}\begin{bmatrix} 1 \\ 0 \end{bmatrix}(v_{s\alpha} - \hat{\omega}(L_d - L_q)i_{s\beta}) \quad (6)
\end{aligned}
$$

$$
\begin{aligned}
\frac{d}{dt}\begin{bmatrix} \hat{i}_{s\beta} \\ \hat{e}_{s\beta} \end{bmatrix} &= \frac{1}{L_d}\begin{bmatrix} -R_s & -1 \\ 0 & 0 \end{bmatrix}\begin{bmatrix} \hat{i}_{s\beta} \\ \hat{e}_{s\beta} \end{bmatrix} + \begin{bmatrix} k_{\beta 1} \\ k_{\beta 2} \end{bmatrix}\tilde{i}_{s\beta} \\
&+ \frac{1}{L_d}\begin{bmatrix} 1 \\ 0 \end{bmatrix}(v_{s\beta} + \hat{\omega}(L_d - L_q)i_{s\alpha}) \quad (7)
\end{aligned}
$$

where $\tilde{i}_{s\alpha} = \hat{i}_{s\alpha} - i_{s\alpha}$, $\tilde{i}_{s\beta} = \hat{i}_{s\beta} - i_{s\beta}$. It leads to the following linear dynamic for the estimation errors :

$$
\begin{aligned}
\frac{d}{dt}\begin{bmatrix} \tilde{i}_{s\alpha} \\ \tilde{e}_{s\alpha} \end{bmatrix} &= \begin{bmatrix} k_{\alpha 1} - \frac{R_s}{L} & -\frac{1}{L} \\ k_{\alpha 2} & 0 \end{bmatrix}\begin{bmatrix} \tilde{i}_{s\alpha} \\ \tilde{e}_{s\alpha} \end{bmatrix} \\
\frac{d}{dt}\begin{bmatrix} \tilde{i}_{s\beta} \\ \tilde{e}_{s\beta} \end{bmatrix} &= \begin{bmatrix} k_{\beta 1} - \frac{R_s}{L} & -\frac{1}{L} \\ k_{\beta 2} & 0 \end{bmatrix}\begin{bmatrix} \tilde{i}_{s\beta} \\ \tilde{e}_{s\beta} \end{bmatrix}
\end{aligned}
$$

where $\tilde{e}_{s\alpha} = \hat{e}_{s\alpha} - e_{s\alpha}$, $\tilde{e}_{s\beta} = \hat{e}_{s\beta} - e_{s\beta}$. A classical pole-placement technique determine the observer gains $(k_{\alpha 1}, k_{\alpha 2}, k_{\beta 1}, k_{\beta 2})$ so that the estimation error vanishes (stable system) without increasing the noise sensitivity impact. The poles are selected in order to have the same dynamics as the Extended EMF when the PMSM operates at the nominal speed.

For the digital implementation, the PMSM is supposed to be isotropic $(L_d = L_q)$. The continuous state space model is linear and stationary, therefore it can be discretized by an exact matrix exponential [19], [20].

2) Adaptive observer: The AO is based on (5) with the assumption that $(L_d = L_q)$. Therefore, the EEMF estimates are expressed as follows :

$$
\begin{aligned}
\dot{e}_{s\alpha} &= -\omega\, e_{s\beta} \\
\dot{e}_{s\beta} &= \omega\, e_{s\alpha}
\end{aligned} \quad (8)
$$

From (8), the adaptive observer is designed as

$$
\begin{aligned}
\dot{\hat{e}}_{s\alpha} &= -\hat{\omega}\,\hat{e}_{s\beta} - L(\hat{e}_{s\alpha} - \hat{e}_{s\alpha}) \\
\dot{\hat{e}}_{s\beta} &= \hat{\omega}\,\hat{e}_{s\alpha} - L(\hat{e}_{s\beta} - \hat{e}_{s\beta})
\end{aligned} \quad (9)
$$

where L is a positive observer gain. The observer (6, 7) is used in order to estimate the back-EMF $(\alpha\beta)$ components. These estimations are used as measurement inputs for the adaptive observer. The error dynamics are given as :

$$
\begin{aligned}
\dot{\tilde{e}}_{s\alpha} &= -\tilde{\omega}e_{s\beta} - L\tilde{e}_{s\alpha} \\
\dot{\tilde{e}}_{s\beta} &= \tilde{\omega}e_{s\alpha} - L\tilde{e}_{s\beta}
\end{aligned} \quad (10)
$$

where $\tilde{e}_{s\alpha} = \hat{\hat{e}}_{s\alpha} - \hat{e}_{s\alpha}$, $\tilde{e}_{s\beta} = \hat{\hat{e}}_{s\beta} - \hat{e}_{s\beta}$ in this sub-paragraph. To guarantee the stability of the above error system, consider the function $V = \frac{1}{2}(\tilde{e}_{s\alpha}^2 + \tilde{e}_{s\beta}^2 + \tilde{\omega}^2)$. The derivative of V becomes :

$$
\dot{V} = -L(\tilde{e}_{s\alpha}^2 + \tilde{e}_{s\beta}^2) + \tilde{\omega}\dot{\tilde{\omega}} + \tilde{\omega}(-\tilde{e}_{s\alpha}\hat{e}_{s\beta} + \tilde{e}_{s\beta}\hat{e}_{s\alpha})
$$

where $\tilde{\omega} = \hat{\omega} - \omega$. To make $\dot{V} < 0$, we must cancel the last two terms (with the assumption that the speed varies slowly $\dot{\omega} = 0$ in contrast with electrical variables). The adaptive law is chosen as $\dot{\hat{\omega}} = \tilde{e}_{s\alpha}\hat{e}_{s\beta} - \tilde{e}_{s\beta}\hat{e}_{s\alpha}$. For the digital implementation, the integral term is discretized by an Euler backward transformation [20]. Moreover, a proportional term is added in order to increase the tracking capabilities during transients. Figure 1 represents the back-emf adaptive observer structure.

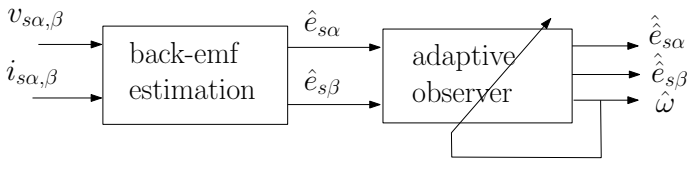

Fig. 1. Back-emf adaptive Observer diagram

C. Simulation and experimental results

The nominal controller based on the standard vector control and the two observers are implemented under Matlab-Simulink® and downloaded in a dSpace® 1104 board. When the estimated variables (computed by the observers) are not used in the controller, this mode is called "open loop" and the mechanical sensor feeds the controller. The top curves in Figs. 2 and 3 show respectively the performances of the speed and position tracking capabilities of the two-stage EKF and the adaptive observer compared to the sensor output. The lower curves represent the speed and position errors compared to the measured variables. The performances are globally satisfactory but can be improved.

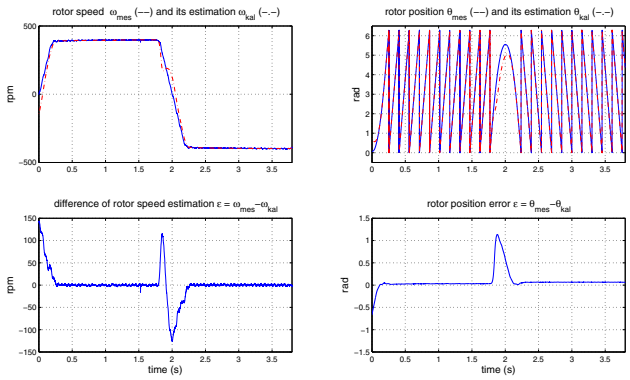

Fig. 2. Experimental results for the OTSEKF in open loop configuration.

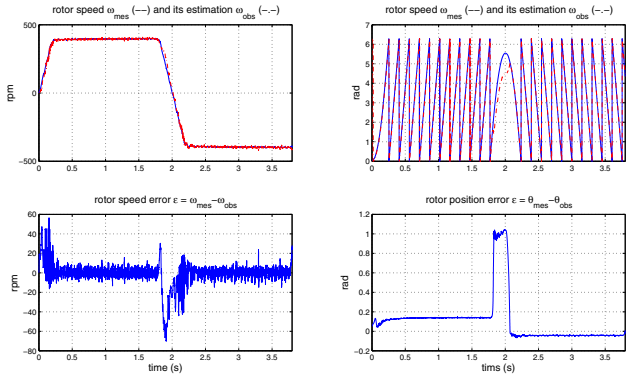

Fig. 3. Experimental results for the AO in open loop configuration.

Intensive simulations are performed to evaluate the robustness of both observers to the stator resistance variation on the whole operating range in the torque-speed frame. From Figs. 4 to 6, we can deduce that for a variation of $\pm 50\%$ of the stator resistance, the steady state speed and position errors are negligible and are symmetrical with the speed. We can conclude that both observers reveal a good robustness.

However, in order to implement the fault tolerant controller, the robustness of the observers needs to be evaluated also during the transients. This analysis is mandatory to extract for each observer the reliability coefficients required by the voting algorithm. Fig. 7 shows the evolution of the errors on the speed range for a resistance detuned of $+50\%$ from the nominal value. From these results, we can conclude the Back-EMF Adaptive Observer exhibits better performances and robustness at medium and high speed and is also less sensitive to stator resistance variation. Which means that in the medium to high-speed range, higher reliability coefficients will be attributed to the Back-EMF AO compared to the EKF.

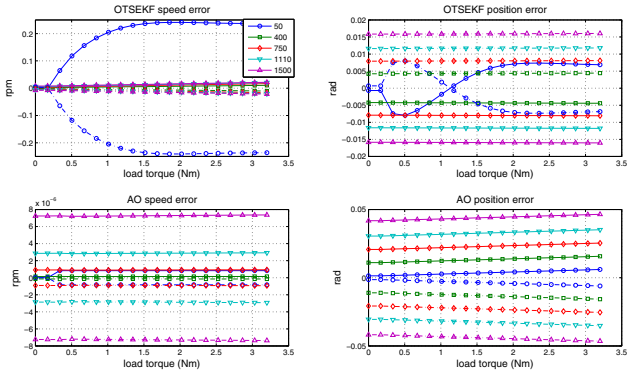

Fig. 4. Steady state speed and position errors ($R_s = R_{snom}$).

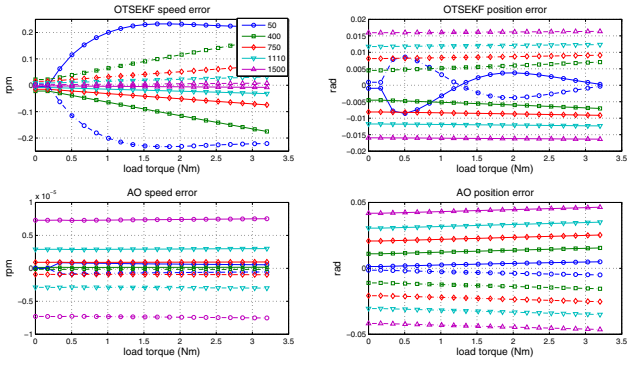

Fig. 5. Steady state speed and position errors ($R_s = 1.5R_{snom}$).

III. Fault-tolerant control

Apart from faults arising in the machine or inverter, the drive is sensitive to fault in different sensors that provide information used by the control system. For a PMSM drive, these sensors typically measure phase currents (at least two of the three phase currents are measured), dc-link voltage (since it is prone to variation), and rotor position. The loss of a sensor leads to unsatisfactory or dangerous behaviour if no mitigation action has been forecast. In the following section, we focus only on mechanical sensors.

A. Position sensor faults

A 12-bit absolute encoder is used as position sensor in this application and can exhibit the following fault conditions [3] :

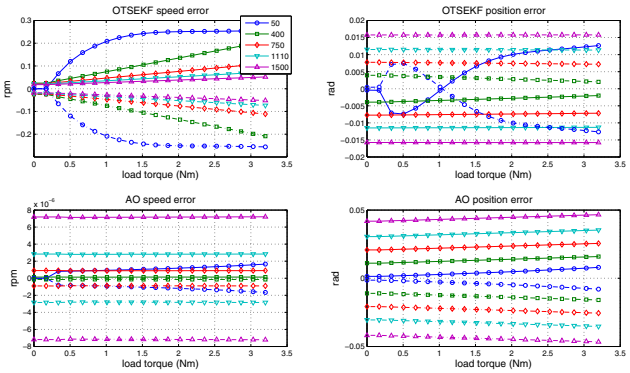

Fig. 6. Steady state speed and position errors ($R_s = 0.5R_{snom}$).

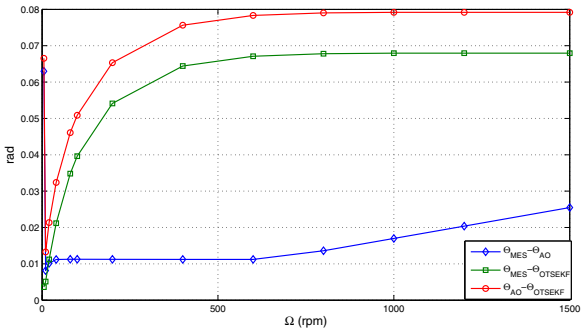

Fig. 7. Estimation error during transient with ($R_s = 1.5R_{snom}$).

- Intermittent sensor connection (F_1),
- Complete sensor outage (F_2),
- DC Bias in sensor measurement (F_3),
- Sensor gain drop (F_4),

The most severe faults are F_1 and F_2 [3], since they imply a momentary or complete lack of information. Potential closed-loop instability could appear if no proper action is undertaken. To increase the reliability of the drive, the controller must accommodate the fault and be able to operate without the mechanical sensor.

B. Absolute encoder faults simulation

One type of absolute encoder failure is presented in this paper : complete sensor outage in the event of a power failure.

The top and bottom curves of Fig. 8-a show respectively the real position, the encoder output and the quantification error. Fig. 8-b represents the same data in case of a complete sensor outage at 0.02s. We can notice the important errors due to the faults. The speed derivation from the position will worsen the impact on the drive if a fault tolerant controller forecasts no mitigation action.

C. Fault-tolerant controller

The structure of the FTC is shown in Fig. 9. The voting algorithm in the control decision block computes the most accurate information (speed and position) from the inputs

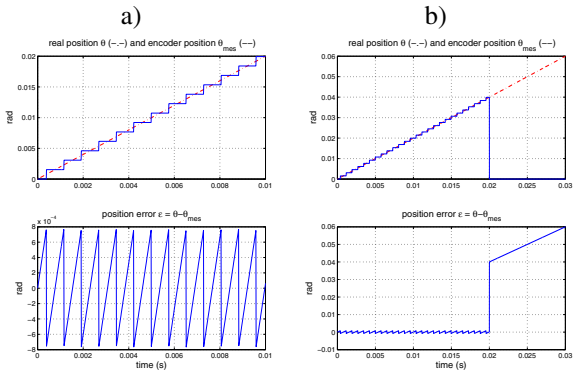

Fig. 8. Position got from encoder and real position in the normal case and in the event of a power failure.

of the sensor and the observers. The control decision block relies on a voting algorithm type in which the emerging output has the highest approval. Several voting techniques have been described in the literature of which the inexact majority [23], and weighted average voters [24] are widely used in control and safety-critical applications. Inexact majority voters produce an output from redundant inputs if there is agreement between a majority number of voter inputs. Weighted average voters always produce an output regardless of the agreement, or otherwise, between redundant inputs by amalgamating the inputs. A major difficulty with inexact majority voters is the need to choose an appropriate threshold value, which has a direct impact on the voter performance. The weighted average voters suffers from a lack of accuracy in normal conditions, i.e. without a fault, because the measured position and speed are mixed with those of the observers producing less accurate values. The other method which is used here is the Maximum Likelihood voting algorithm [25] in which a probability χ_j for each input j is computed based on reliability coefficients. The computation of the probability coefficients that the output j is correct is slightly modified to introduce a threshold and in normal operating conditions to choose the position sensor as the emerging output :

$$\chi_j = \prod_{i=1}^{N} \Delta_j(i) \Big/ \sum_{k=1}^{N} \prod_{i=1}^{N} \Delta_k(i)$$

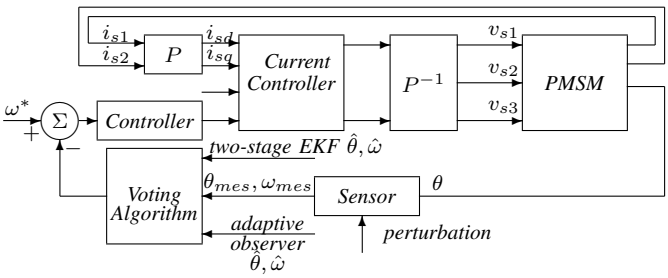

Fig. 9. Fault tolerant controller structure.

with

$$\Delta_k(i) \quad = \quad \begin{cases} f_k & \text{if } |x_i - x_k| \leq D_{max_{ik}} \\ \frac{1-f_k}{N-1} & \text{else} \end{cases}$$

After extensive simulations, the threshold $D_{max_{ik}}$ is set to 0.1 rad at zero speed and to 0.15 at the nominal speed. The reliability coefficients determined over the whole speed range for each observer are set as follows :

- 0.96 at zero speed to 0.92 at the nominal speed for the OTSKE,
- 0.92 at zero speed to 0.96 at the nominal speed for the Back-emf AO,
- A constant reliability coefficient (0.99) for the speed sensor.

To evaluate the fault tolerant controller, a position sensor failure (event of a power failure) and recovery is introduced between $1.5 \rightarrow 2.5$s, $3.8 \rightarrow 4.5$s, $5.5 \rightarrow 6,5$s, $7.5 \rightarrow 8.5$s and $9.8 \rightarrow 10.5$s. Fig. 10 shows the response of the fault tolerant controller. At low and medium speed, the OTSEKF output is selected in the case of failure. At high speed, it is the AO output which is engaged to maintain the level of performance. The position and speed estimation error is evaluated as the difference between the real position and speed (non erroneous measured speed) and the emerging outputs of the voting algorithm.

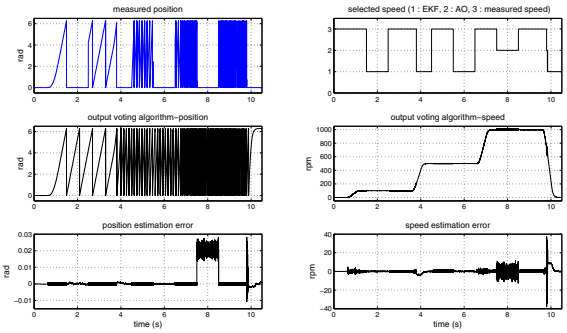

Fig. 10. Simulation results in the event of a power failure.

IV. Conclusion

This paper has described a fault-tolerant control system for a high-performance PMSM drive. The FTC is an observer-based structure with a voting algorithm, which selects the appropriate speed and position in case of mechanical sensor failure from two observers. An EKF and a Back-emf AO have been designed and evaluated off line with experimental data. They also exhibit good robustness against stator resistance variation. The transient behaviour of both observers are analysed to extract the reliability coefficients required by the Maximum Likelihood voting algorithm. Finally the FTC feasibility has been proven in case of an absolute encoder failures (complete outage and bit errors) and recovery on the whole speed range.

References

[1] Z. Q. Zhu, D. Howe, "Electrical machines and drives for electric, hybrid, and fuel cell vehicles," *Proceedings of the IEEE*, Vol. 95, N°4, April 2007, pp. 746-765.

[2] B. K. Bose, "Modern power electronics and AC drives," *Prentice Hall*, New Jersey, 2002.

[3] D. U. Campos-Delgado, E. Palacios, D. R. Espinoza-Trejo, "Fault-tolerant control in variable speed drives : a survey" *IET Electric Power Applications*, Vol. 2, Issue2, Mars 2008, pp. 121-134.

[4] D. Diallo, M. E. H. Benbouzid, A. Makouf, "A fault-tolerant control architecture for induction motor drives in automotive applications," *IEEE Transactions on Vehicular technology*, Vol. 53, N°6, 2004, pp. 1847-1855.

[5] Y. S. Jeong, S. K. Sul, S. E. Schulz. N. R. Patel, "Fault detection and fault-tolerant control of interior permanent-magnet motor drive system for electric vehicle, "*IEEE Transactions on Industry Applications*, Vol. 41, N°1, January-February 2005, pp. 46-51.

[6] G. Bisheimer, C. De Angelo, J. Solsona, G. Garcia, "Sensorless PMSM drive with tolerance to current sensor faults," *IEEE International Conference on Industrial Electronics IECON*, Orlando, USA 2008.

[7] O. Wallmark, L. Harnefors, O. Carlson, "Control algorithms for a fault-tolerant PMSM drive," *IEEE Transactions on Industrial Electronics*, Vol. 54, N°4, 2007, pp. 1973-1980.

[8] M. Hilairet, M. E. H. Benbouzid, D. Diallo, "A Self-Reconfigurable and Fault-Tolerant Induction Motor Control Architecture for Hybrid Electric Vehicles," *IEEE, International Conference on Electrical Machines, ICEM06*, Chania, Greece, 2006.

[9] M. J. Corley, R. D. Lorenz, "Rotor Position and Velocity Estimation for a Salient-Pole Permanent Magnet Synchronous Machine at Standstill and High Speeds," *IEEE Transactions on Industry Applications*, Vol. 34, N°4, 1998, pp. 784-789.

[10] A. Consoli, G. Scarcella, A. Testa, "Industry Application of Zero-Speed Sensorless Control Techniques for PM Synchronous Motors," *IEEE Transactions on Industry Applications*, Vol. 37, N°2, 2001, pp. 513-521.

[11] Y. H. Kim, Y. S. Kook, "High Performance IPMSM Drives without Rotational Position Sensors Using Reduced-Order EKF," *IEEE Transactions on Energy Conversion*, Vol. 14, N°4, 1999, pp. 868-873.

[12] G. Zhu, A. Kaddouri, L.A. Dessaint, O. Akhrif, "A Nonlinear State Observer for the Sensorless Control of a Permanent-Magnet AC Machine," *IEEE Transactions on Industry Electronics*, Vol. 48, N°6, 2001, pp. 1098-1108.

[13] P. P. Vas, "Sensorless vector and direct torque control," *Oxford University Press*, 1998.

[14] M. S. Grewal, A. P. Andrews, "Kalman filtering, theory and practice," *Prentice Hall*, Englewood Cliffs, New Jersey, 1993.

[15] C. S. Hsieh, F. C. Chen, "Optimal solution of the two-stage Kalman estimator," *IEEE Transactions on automatic control*, Vol. 44, N°1, 1999, pp. 194-199.

[16] A. Akrad, M. Hilairet, D. Diallo, "A sensorless PMSM drive using a two stage extended Kalman estimator, " *IEEE International Conference on Industrial Electronics IECON*, Orlando, USA 2008.

[17] M. Hilairet, E. Berthelot, F. Auger, "Speed and rotor flux estimation of induction machines using a two-stage extended Kalman filter, " *Automatica*, accepted for publication as regular paper, 2009.

[18] Z. Chen, M. Tomita, S. Doki, S. Okuma, "An Extended Electromotive Force Model for Sensorless Control of Interior Permanent Magnet Synchronous Motors," *IEEE Transactions on Industry Electronics*, Vol. 50, N°2, 2003, pp. 288-295.

[19] Z. Boulbair, M. Hilairet, F. Auger, L. Loron, "Sensorless Control of a PMSM Using an Efficient Extended Kalman Filter," *International Conference of Electrical Machines ICEM04* ,Cracovie, Pologne, 2004.

[20] W. Levine, "The control handbook," CRC Press.

[21] B. Nahid-Mobarakeh, F. Meibody-Tabar, F. Sargos, "Mechanical sensorless control of PMSM with online estimation of stator resistance, "*IEEE Transactions on Industry Applications*,Vol. 40, N°2, March/April 2004, pp. 457-471.

[22] C. W. De Silva, "Mechatronics: An Integrated Approach,"*CRC Press*, 2005.

[23] J.M. Bass, P.R. Croll, P.J. Fleming, L.J.C. Woolliscroft, "Three Domain Voting In Real-time Distributed Control Systems," *2nd Euromicro Workshop on Parallel and Distributed Processing*, 1994, pp. 317-324.

[24] G. Latif-Shabgahi, J.M. Bass, S. Bennett, "History-based weighted average voter: a novel software votingalgorithm for fault-tolerant computer systems," *Proceedings. Ninth Euromicro Workshop on Parallel and Distributed Processing*, 2001, pp. 402-409.

[25] Y. Leung, "Maximum likelihood voting for fault-tolerant software with finite output-space ," *IEEE Transactions on Reliability*, Vol. 14, N°3, 1995, pp. 419-427.